Transition from Townsend to radio-Frequency homogeneous dielectric barrier discharge in a Roll-to-Roll configuration

Rémy Bazinette, Jean Paillol, Françoise F. Massines

▶ **To cite this version:**

Rémy Bazinette, Jean Paillol, Françoise F. Massines. Transition from Townsend to radio-Frequency homogeneous dielectric barrier discharge in a Roll-to-Roll configuration. Journal of Applied Geophysics, 2016, 119 (24), ⟨10.1063/1.4953389⟩. ⟨hal-01466769⟩

HAL Id: hal-01466769

https://univ-perp.hal.science/hal-01466769v1

Submitted on 28 Aug 2024

HAL is a multi-disciplinary open access archive for the deposit and dissemination of scientific research documents, whether they are published or not. The documents may come from teaching and research institutions in France or abroad, or from public or private research centers.

L'archive ouverte pluridisciplinaire **HAL**, est destinée au dépôt et à la diffusion de documents scientifiques de niveau recherche, publiés ou non, émanant des établissements d'enseignement et de recherche français ou étrangers, des laboratoires publics ou privés.

HAL Authorization

Transition from Townsend to radio-Frequency homogeneous dielectric barrier discharge in a Roll-to-Roll configuration

R. Bazinette[1,2], J. Paillol[2], F. Massines[1]

[1] CNRS-PROMES, Rambla de la Thermodynamique, 66100, Perpignan, France
Telephone: +33(0)468682228; Fax: +33(0)468682213
email: francoise.massines@promes.cnrs.fr
[2] SIAME, Université de Pau et des Pays de l'Adour, 64012, Pau, France

Abstract: The aim of this paper is to better understand the transition from Townsend to radio-frequency homogeneous dielectric barrier discharge (DBD) at atmospheric pressure. The study is done in an Ar/NH_3 Penning mixture for an electrode configuration adapted to roll-to-roll plasma surface treatment. The study was led in a frequency range running from 50 kHz up to 8.3 MHz leading to different DBDs modes with a 1 mm gas gap: Glow (GDBD), Townsend (TDBD) and Radio-frequency (RF-DBD).

In the frequency range between TDBD and RF-DBD, from 250 kHz to 2.3 MHz, additional discharges are observed outside the inter-electrode gas gap. Because each high voltage electrode are inside a dielectric barrel, these additional discharges occurs on the side of the barrel where the gap is larger. They disappear when the RF-DBD mode is reach in the 1 mm inter-electrode gas gap i.e. for frequencies equal or higher than 3 MHz.

Fast imaging and optical emission spectroscopy show that the additional discharges are radio-frequency DBD while the inter-electrode discharge is a TDBD. The RF-DBD discharge mode is reach when electrons drift becomes low enough compare to the voltage oscillation frequency to limit electrons loss at the anode. To check that the additional discharges are due to a larger gas gap and a lower voltage amplitude, the TDBD / RF-DBD transition is investigated as a function of the gas gap and the applied voltage frequency and amplitude. Results show that the increase of the frequency at constant gas gap or of the gas gap at constant frequency allows to obtain RF-DBD instead of TDBD. At low frequency and large gap, the increase of the applied voltage allows RF-DBD / TDBD transition.

As a consequence, an electrode configuration allowing different gap values is a solution to successively have different discharge modes with the same applied voltage.

Keywords: dielectric barrier discharge (DBD), atmospheric pressure, glow, Townsend-like, radio-frequency, emission spectroscopy, continuum, argon,

1. Introduction

Homogeneous dielectric barrier discharges (DBD) at atmospheric pressure offer a suitable plasma technology for continuous-feed thin film deposition processes [1]. The most widely used configuration for roll-to-roll treatment consists of injecting reactive gases between two insulating tubes that contain high-voltage electrodes. The tubes face the substrate, which is layered directly onto a grounded roll. The advantage of this configuration is that it generates two linear plasma area that can easily be stretched out to fit the width of the substrate. This continuous-feed in-line technique can be scaled to easily treat many square kilometers of material. The solution already works well for surface activation, but is still in pre-industrial stage for deposition processes.

The quality of the thin film coating obtained is satisfactory, but the power obtained by homogeneous DBDs with a sinusoidal voltage in a frequency range from 1 to 200 kHz is limited to around 1 W/cm^3. This power is too low to efficiently dissociate the thin film precursors. The power is thus the leading limiting factor for thin-film deposit rate. Different solutions for increasing discharge power have been investigated, including glow-like discharge [2], square-wave current-powered Townsend-like DBDs (TBDB) [3] and radio-frequency discharges (RF–DBD) [2,4,5]. The first two solutions are based on highly specific discharge power supplies, whereas regular commercially available power supply systems can be used to increase discharge excitation frequency. To use radio-frequency for discharge enables a change in mechanism of ionization because ions and a fraction of electrons are trapped in the gap.

The ionization mechanisms of homogeneous atmospheric-pressure RF-DBD are similar to low-pressure discharges [4,5]. Alpha-mode discharge with in-gas ionization and gamma-mode discharge with substantial secondary electron emission are observed [4]. Either way, at atmospheric pressure, there is generally a greater degree of ionization in the gas bulk than at low pressure [6]. This come from the more intensive ion-electron recombination linked to the shorter mean free paths of the atomic species. Most of the relevant published researches use excitation frequencies that are constrained by commercially available power-supply systems, typically 13.56 MHz [7,8].

As the frequency increases from 100 kHz to a few MHz, the discharge goes through major physical transitions. The ions get increasingly trapped into the gap up to a point where they no longer oscillate under the effect of applied voltage polarity change [9]. Transition from pulsed to continuous-mode is also observed [10]. Recent work [11,12] using an argon ammonia Penning mixture demonstrated the influence of excitation frequency on broadband DBD modes between 50 kHz and 8.3 MHz. This study demonstrated that with a 1 mm gas gap, the discharge is in a glow-mode (GDBD) up to 200 kHz, then in a Townsend-like mode (TDBD) from 250 and 550 kHz and in a radio-frequency mode (RF-DBD) beyond 3 MHz when electron trapping begins. The transition from glow-mode to Townsend-mode is fairly clear. However, between Townsend mode and radio-frequency mode, there is a strong drop in discharge intensity before the RF mode is established. This work focuses on this transition domain.

In RF-DBD, the mean power is about 30 W/cm^3 [11]. This increase in power is associated with a 6-fold decrease in breakdown voltage, which is in agreement with the concomitant two orders of magnitude increase in electron density. The transition from TDBD to RF-DBD therefore induces a decrease in mean electron energy that reflects a change of ionization mechanism. Cathode secondary electron emission gives way to electron acceleration by the cathode sheath. In the alpha-mode RF-DBD, ionization in the

plasma bulk dominates, with cold electrons in the gas bulk and electrons being heated by sheath oscillations at the sheath edges [6]. The discharge produced is relatively unaffected by the type of surface it interacts with, which is a strong benefit for an in surface treatment usage. This alpha-mode RF-DBD can become gamma-mode if the driving voltage is sharply increased. The alpha-to-gamma transition is associated with a strong increase in secondary electron emission [7] and a dominant role of the sheaths over the bulk, which translates into light emission in the vicinity of the dielectric surfaces.

The purpose of this work is to gain a more thorough understanding of the mechanisms controlling the transition from the TDBD to the RF-DBD mode by investigating the light emitted by the discharges in a specific configuration adapted to continuous-feed roll-to-roll plasma surface treatment. Here, the gas is injected between the two discharge zones generated by applying high voltage to the electrodes inside alumina square tubes. The main advantage of this configuration is that scale-up only requires an extension of the tubes. As the TDBD to RF-DBD transition is linked to electron and ion trapping in the gas gap, the three parameters studied are excitation frequency, voltage amplitude, and gas gap. Voltage frequency is the variable that defines the period during which charged particles are accelerated in the same direction. Voltage amplitude is the variable that defines their acceleration. Gas gap is the variable that defines the maximum path distance travelled by electrons before hitting a wall. As gas density is a fixed variable, those three parametres only will affect losses on the walls. Here, the experimental apparatus is described, and then the results are reported and discussed.

2. Experimental

Figure 1 is a schematic diagram of the discharge cell. The discharge cell is composed of a pair of high-voltage electrodes able to generate two 14×50 mm² discharge zones of 2 mm thick. Each electrode is produced by metalizing one of the inner faces of an alumina (dielectric material) square tube with 3 mm thick walls and rounded-off corners.

The ground electrode is at the opposite side of the gas gap. It is a 50×50 mm² surface metalized onto the rear face of a 70×70 mm² alumina plate. The inter-electrode gas gap can be adjusted from 1 to 4 mm. This configuration is widely used in industry-scale reactors for roll-to-roll corona treatment [13,14].

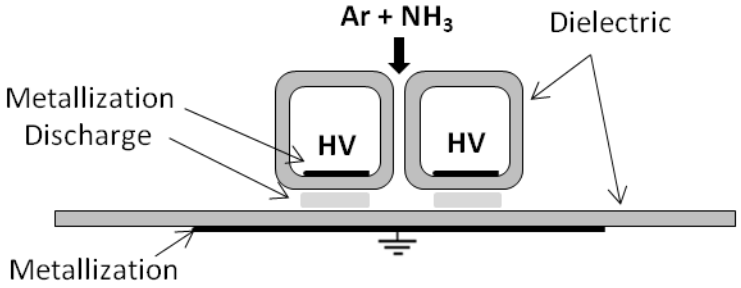

Figure 1: Schematic diagram of the discharge cell

The discharge cell is inside a closed reactor. Before igniting the discharge, the ambient air is eliminated by a primary vacuum and then the reactor is filled to atmospheric pressure (760 Torr) with Alphagaz 2 argon (Air Liquide). The Ar/NH_3 mixture is introduced through the 1.5×50mm² injection slit located between the two alumina tubes housing the high-voltage electrode. The argon flow rate is 3 L/min and the NH_3 concentration is 133 ppm. This configuration ensures a laminar flow of gas between the

electrodes [15].

The electrical circuit feeding the pair of high-voltage electrodes delivers a sinusoidal voltage [11]. It is composed of a waveform generator connected to a PRANA GN500 broadband power amplifier working in the 100 kHz–200 MHz range. Since the voltage at the amplifier output is not strong enough to ignite discharge at atmospheric pressure, the amplifier output is connected to a homemade transformer which increases voltage amplitude while matching the discharge cell impedance near 50 Ω. Specifically, the target frequency depends on the discharge cell capacitance which corresponds to the equivalent capacitance of the two electrodes covered by a solid dielectric material and separated by the gas gap. The order of magnitude of this capacitance is 10 pF (C_{DBD}). This capacitance and the transformer secondary coil form a RLC circuit oscillating with a natural frequency for which the power transferred and the applied voltage are maximal. At the resonance frequency, reflected power is minimal as the impedance match with the amplifier is optimal. This frequency is obtained experimentally by tuning the frequency of the waveform generator to the natural resonant frequency of the RLC circuit. The use of different transformers makes possible the test of a large number of frequencies in a very broad domain spanning 140 kHz to 9.6 MHz.

Another electrical circuit is used to work at frequencies from 40 to 60 kHz. This circuit involves much the same principle-a waveform generator is used with a Crest Audio CC4000 power amplifier connected to a transformer which supplies the voltage to the electrodes. However, in this configuration, the secondary circuit can operate outside of the resonance frequency. Both current amplitude and frequency are then separately tunable.

The electrical measurements are performed using a current probe (LILCO LTD 13W5000) and a voltage probe (Tektronic P6015A) connected to an oscilloscope (Tektronix DPO4104 1 GHz).
Discharges were photographed using a PI-MAX II intensified CCD camera (Princeton Instruments) with a lens working in a 200 to 900 nm response window and optimized for the UV range. Integration time down to 5 ns is used to track the discharge over time by synchronizing the camera with the waveform generator synchronization signal.
UV-VIS optical emission spectrometry (OES) with a long exposure time (100 ms) was performed with a Maya2000Pro spectrometer (Ocean Optics) system working at a 14 µm pixels size, a 25 µm slit width, and a 600 µm-diameter optical fiber. The spectrometer and the optical fiber was intensity-calibrated from 220 to 1100 nm with a DH2000-CAL (Ocean Optics) calibration light source.

3. Results

First, discharge modes as a function of frequency are presented in order to highlight the different operating domains. Next, the discharge pattern over a one voltage cycle scale is shown as a function of frequency. Fast imaging and optical emission spectroscopy were used to identify the discharges observed during the transition. Finally, the effect of increasing the gas gap and the applied voltage on the resulting transition is shown.

3.1 Discharge modes as a function of frequency

We had previously [11] identified the different DBDs observed in the inter-electrode gap between 50 kHz to 8.3 MHz. This identification is based on the spatial distribution of light across the inter-electrode gap at the maximum discharge light. Light emission is maximal at i) the cathode in GDBD, ii) the anode in TDBD, iii) the center in RF-DBD. The discharges remain homogeneous, i.e. free of micro-discharge, whatever the excitation frequency.

In the same frequency range, the discharges were photographed using a CCD camera with a 3 ms integration time in order to highlight the changes in spatial distribution of the discharge light emission in the discharge cell (Figure 2). From 50 kHz to 1.5 MHz, both the high-voltage electrodes are connected. Beyond 2.3 MHz, only the left-side electrode is connected.

Discharge regime	Frequency	Picture		Scale	Maximum intensity (a.u.)
		Left electrode	Right electrode		
GDBD	50 kHz	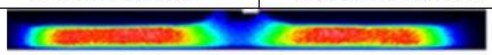		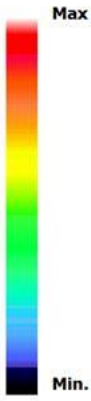	5922
TDBD	250 kHz	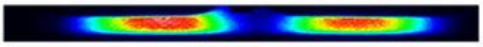			3245
	550 kHz				2168
Transition	800 kHz				1683
	1.5 MHz	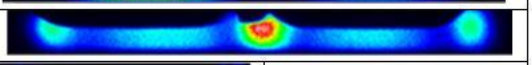			1410
	2.3 MHz				1676
RF-DBD	4.4 MHz	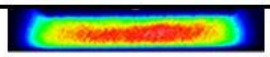			14717
	8.3 MHz	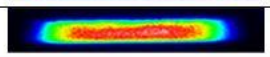			15936

Figure 2: Discharge photographed with a long (3 ms) exposure time for different frequencies and different discharge regime with a 1 mm gas gap

Figure 2 shows that up to 200 kHz, the homogenous discharge is in a glow mode. The length of the discharge in this mode is similar to the length of the high-voltage electrodes (14 mm). The Townsend mode was clearly identifiable between 250 and 550 kHz. The discharge is choked after 9 mm towards the exits of the electrodes (9 mm). Increasing the voltage does not lengthen the homogeneous discharge zone. If the voltage increases enough to ignites the discharges beyond 9 mm, it is unstable and filamentary. This observation is attributed to discharge-driven dissociation of NH_3 that leaves too few NH_3 at the exit for Penning ionization ($Ar(^3P_2) + NH_3 \rightarrow NH_3^+ + e + Ar$ [16]) to create enough electrons. Thus, the discharge tends to ignite in streamer mode.

Beyond TDBD mode (> 550 kHz) and before RF-DBD mode (3 MHz), other discharges are observed to appear outside the 1 mm inter-electrode gap. These additional discharges are located on either side of the above-stated discharge zones, in the gas-in and gas-out zones:

i) One is at the center of the system, between the two dielectric bars, in the gas injection

channel, its height is 3 mm.

ii) Two others are at the rounded-off corners of the dielectric bars, towards the end of the gas confinement zone. Their height is about 2 mm.

The light intensity of these additional discharges increases with increasing frequency, while the intensity of the inter-electrode discharge decreases. Another observation is that the breakdown voltage of the additional discharge at the center occur for an applied voltage 50 V higher than the minimum applied voltage leading to the breakdown between the electrodes. When the applied voltage increases, the intensity of all discharges increases as well without any increase in total length of the discharges. At this point, there are still dark zones separating the inter-electrode discharges from the additional discharges that only develop where the gas gap is the larger.
At 2.3 MHz, only the left-hand electrode was connected to the high voltage in order to see how just one electrode contributes to the center located additional discharge. In this configuration, the pair of additional discharges on either side of the inter-electrode discharge are found symmetrical to the electrode midpoint. They also have the same luminous intensity. These additional discharges appear independently of the gas injection system and independently of discharge at the second electrode.

When the inter-electrode discharge changes to RF mode (> 3 MHz), the additional discharges fail to appear, and instead the inter-electrode discharge covers the electrodes entirely, as with a GDBD.

3.2 Characterization of discharges at the TDBD/RF-DBD transition

To better characterize the different discharge modes, emission spectroscopy and imaging are used. The results reported below present the time evolution of the discharges light emission in the TDBD-to-RF-DBD transition domain studied.

3.2.1 Time evolution of the discharges

Time evolution of the discharge was studied using 10 ns exposure photographs over one voltage cycle at different frequencies from 250 kHz to 3 MHz. Figure 3 illustrates the results obtained at 550 kHz and 1.5 MHz. It charts the variation in light intensity of the inter-electrode discharge and additional discharges over one cycle together with photos taken at peak and zero applied voltage. Regardless of the frequency, the inter-electrode discharge stays ignited.

At 550 kHz, the light intensity of the inter-electrode discharge reaches a peak near the anode, which is a characteristic feature of a Townsend discharge [11,17]. Thereafter, light intensity decreases faster at the anode than at the center of the inter-electrode gap. During the next half-cycle, light output intensifies near the new anode. An additional discharge becomes clearly visible around the maximum of the applied voltage, i.e when the high voltage electrode is cathode. It is located between the two high-voltage electrodes, at the gas injection inlet. It has a very short ignition window (450 ns). On the other cycle this additional discharge still occurs but its intensity is so low that it cannot be seen with the intensity scale of figure 3. These discharges are not synchronized with the inter-electrode discharge, which thus confirms that they are not propagated from the inter-electrode discharge but exists as additional independent discharges. Their light output is diffuse, which means they are not filamentary

discharges.

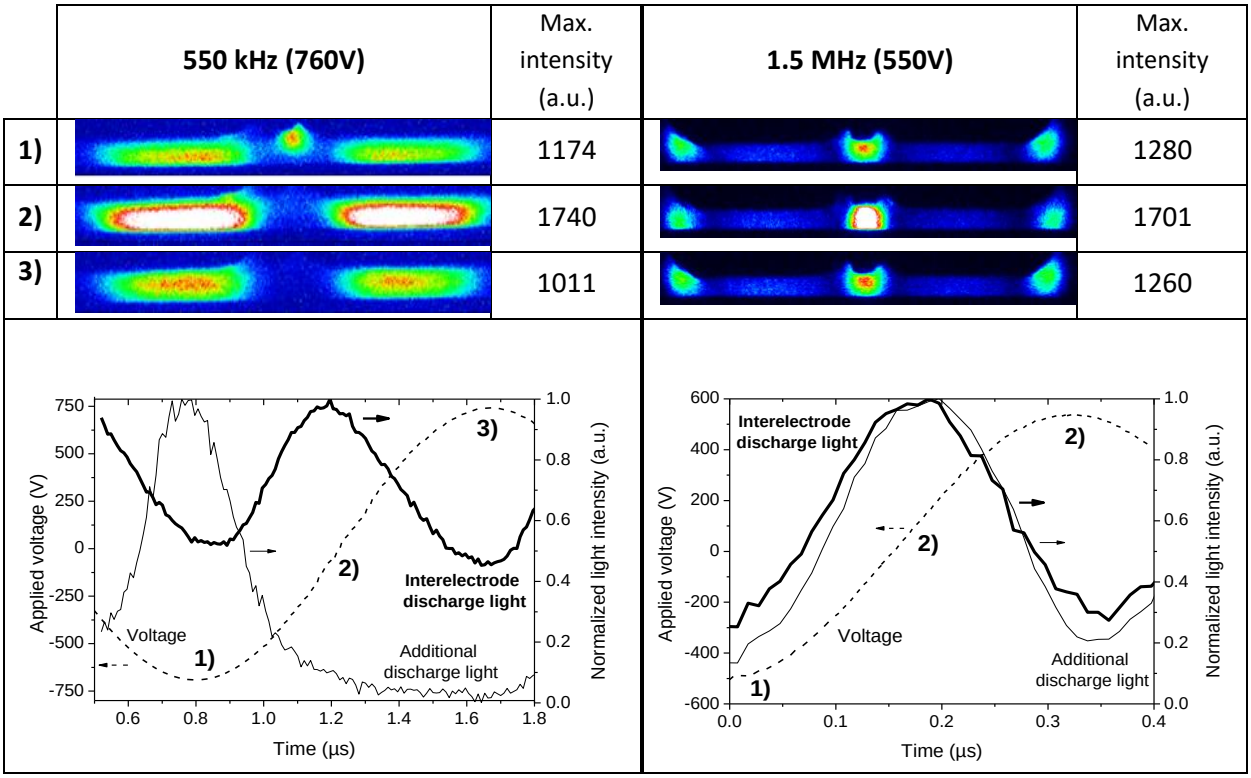

Figure 3: Discharge photographed with a 10 ns exposure time when the applied voltage is equal to zero, 2) and maximum, 1) and 3) at 550 kHz and 1.5 MHz, applied voltage (dash) and discharge light intensity for inter-electrode discharge (thick dash) and center additional discharge (thin dash) *vs* time

At 1.5 MHz, the additional discharges are more intense than the inter-electrode discharge. All discharges stay ignited and in-phase. However, they are systematically split by a dark space.

Observations spanning the whole frequency range under study show that the additional discharges get clearer as excitation frequency gets higher up to 3 MHz:

i) at 250 kHz, the additional discharge is only detectable between the two dielectric bars and during the voltage peak of the negative voltage half-cycle
ii) at 550 kHz, it is visible over both half-cycle in function of applied voltage and it is more intense during the voltage peak of the negative voltage half-cycle
iii) beyond 800 kHz, the other two additional discharges appear either side of the high-voltage electrodes.

Their light intensity increases with frequency, getting higher as the light intensity of the inter-electrode discharge gets lower until 3 MHz. Their emission lifetime also increases with frequency. It grows from 100 ns at 250 kHz to 450 ns at 550 kHz. At higher frequencies, the additional discharge emissions are continuous.

The phase shift between the two discharges has been determined from fast imaging. As illustrated in

Figure 4, it changes radically with excitation frequency. As long as the inter-electrode discharge is Townsend-like, phase shift angle stays at a constant 80°. Beyond 800 kHz, phase shift drops and is equal to zero at 1.2 MHz. The two discharge modes are almost completely out-of-phase up to 800 kHz, whereas beyond 1.2 MHz both discharge emissions are in phase.
To push this analysis further, a series of optical emission spectroscopy measurements were performed.

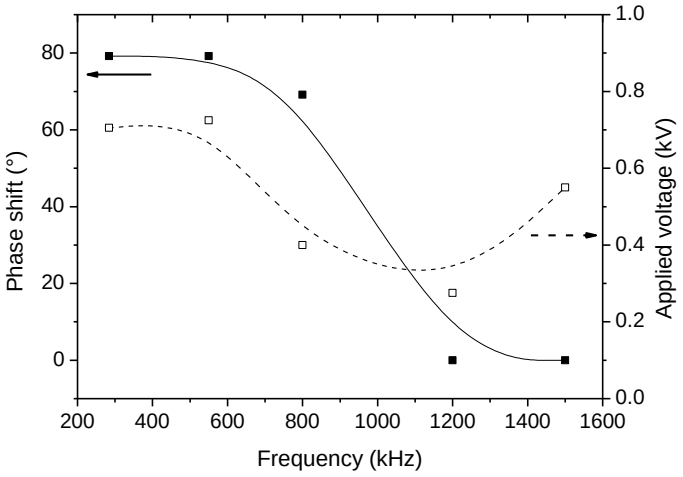

Figure 4: Phase shift between the maximum of the inter-electrode and center additional discharge light and voltage amplitude as a function of frequency, measurements performed on the negative voltage half-cycle.

3.2.2 Optical emission spectroscopy

Optical emission spectroscopy was employed to determine the effective mode of the additional discharges, as low-frequency DBD (GDBD and TDBD) and radio-frequency DBD are known to exhibit very different emission spectra.

The RF-DBD spectrum features a broad emission continuum in the UV–Vis range and very low argon emissions compared to what is observed at low-frequency (LF). Consequently, this continuum is specific to the RF-DBD mode. As shown previously [12], it is related to electron-atom Bremsstrahlung and thus to high electron density [18]. In contrast, the LF discharges are characterized by a spectrum that features a strong argon emission component. The difference between the RF and LF spectrum is largely discussed and correlated to higher electron energy in LF and lower electron energy in RF.

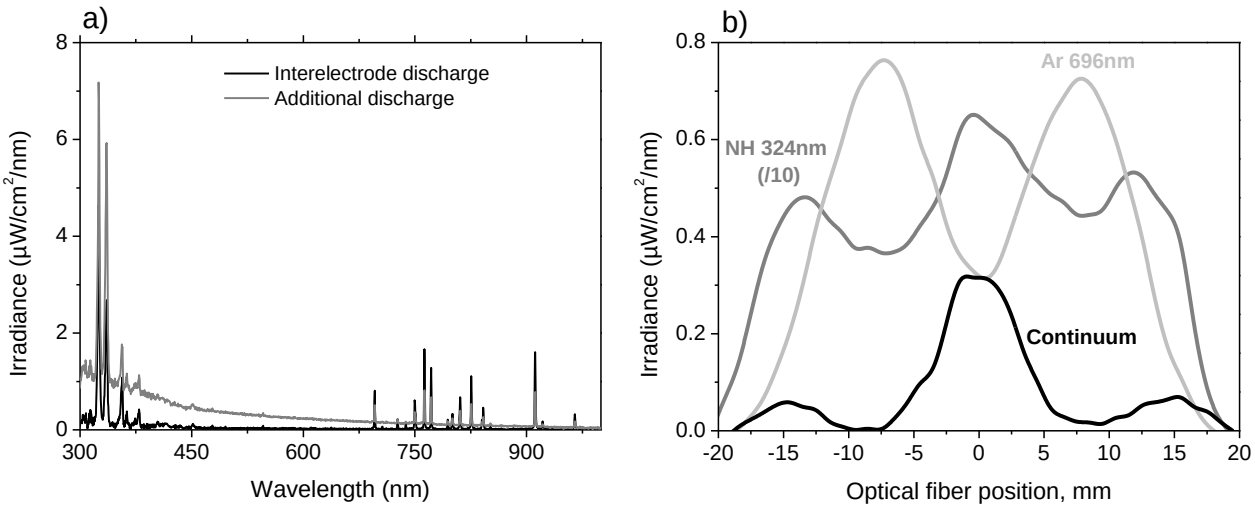

Figure 5: a) Irradiance spectrum of inter-electrode and center additional discharges b) Spatial irradiance profile of the continuum at 500 nm (black line), Ar at 696 nm (light gray) and NH at 324 nm (gray) for 1.5 MHz as a function of optical fiber position in the plasma zones. Zero is the center of the gas injection.

At 550 kHz, the additional discharge at center gives off very little light and has a short lifetime, which makes the signal intensity below the detection level. However, once at 1.5 MHz, it becomes intense enough to be characterizable. Figure 5-a) compares 100 ms integration time irradiance between the inter-electrode discharge under the high-voltage electrodes and the additional discharge at the center position for a driving frequency of 1.5 MHz. Only the additional discharges demonstrate a visible emission continuum. This continuum is comparable to the continuum observed for RF-DBD at 3 MHz. The Ar emission at 696 nm, NH emission at 324 nm and amplitude of the continuum at 500 nm have been plotted (Figure 5-b) as a function of optical fiber position from extreme left to the extreme right of the treatment head. Argon emission is observed to peak under the high-voltage electrodes, i.e. where the electric field is most intense. No continuum is detected in this zone, which makes it a LF-like discharge, i.e. a discharge where there is insufficient electron density to induce a Bremsstrahlung emission. In contrast, in the additional discharges, the comparatively very weak argon emission gives way to the dominant NH and continuum emission components. The additional discharges therefore feature similar to those of RF-DBDs. Consequently, the strong glow of the additional discharges observed in the photographs (Figure 2) is explained by the presence of the continuum.

The additional discharges are similar to RF-DBD observed in a larger gap than the inter-electrode gap in a zone where the electric field is low. In fact the breakdown voltage is slightly higher than the breakdown voltage of the inter-electrode discharge. As the electric field is weaker in these zones, a local build-up of ions and electrons could be enough for the electron density to reach a point where mobile electrons can trigger the formation of a sheath, in turn accelerating the electrons that bounce back. It seems that the amplitude of oscillation of charged species in the alternating electric field likely plays a key role. RF discharge behavior happens when the right frequency/inter-electrode gap/voltage amplitude combination enables the trapping of charged species.
To validate this hypothesis, we studied the discharge emissions in response to variations in gas gap and amplitude of the voltage applied.

3.3 Effect of gas gap and voltage on TDBD/RF-DBD transition

3.3.1 Effect of gas gap

Inter-electrode gaps from 1 to 4 mm were tested. The observations were carried out while keeping driving voltage at the same order of magnitude as previously. When the gap height is increased, the electric field is consequently reduced, which leads to less drift and more trapping of charged species. As previously, fast imaging combined with optical emission spectroscopy were used to characterize the discharges from 250 kHz to 1.5 MHz.

At 250 kHz, inter-electrode discharge shows no change in behavior under the increase of the gap height. Peak light intensity is anode-side. A weak additional discharge is observed for a gas gap of 1 mm if the applied voltage is 760 V. The very weak additional discharges are not detected at gas gaps above 1 mm. The electric field must be too weak.

At 550 kHz, strong variations are observed when the inter-electrode gap is increased. These variations are illustrated in Figure 6 where discharges photographed at 550 kHz and 1.5 MHz are shown for different inter-electrode gap.

Gas gap	550 kHz	1.5 MHz
1 mm	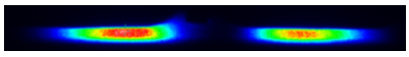	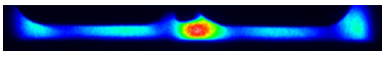
2 mm	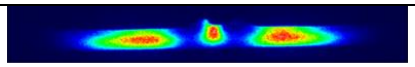	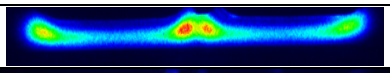
3 mm	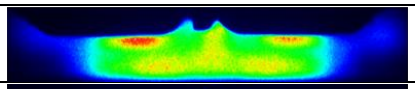	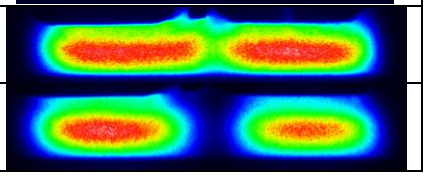
4 mm	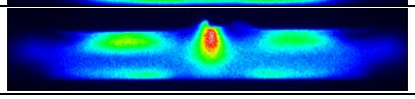	

Figure 6: 3 ms exposure time photographs of discharge at 550 kHz and 1.5 MHz at different inter-electrode gaps (1, 2, 3 and 4 mm)

In TDBD at 550 kHz, the increase in gas gap intensifies the additional discharges, which is consistent with an increase of ions trapping, whereas the inter-electrode discharge remains Townsend-like at gaps from 1 to 3 mm. For 2 mm, the additional discharge at the center appears. It is visible over both half-cycle, and its intensity and lifetime are just as large as the inter-electrode discharge. For a 3 mm gap, additional discharges are observed outside the electrodes. For 4 mm, the three additional discharges are always observed. Whatever the gap, additional discharge and inter-electrode discharge are out of phase. However, in the 4 mm gap, two discharges successively occur. The first is a Townsend and the second one occurs at the same time of the additional discharge and is light is in the middle of the gap. The different discharge modes can be identified from emission spectra. (Figure 7)

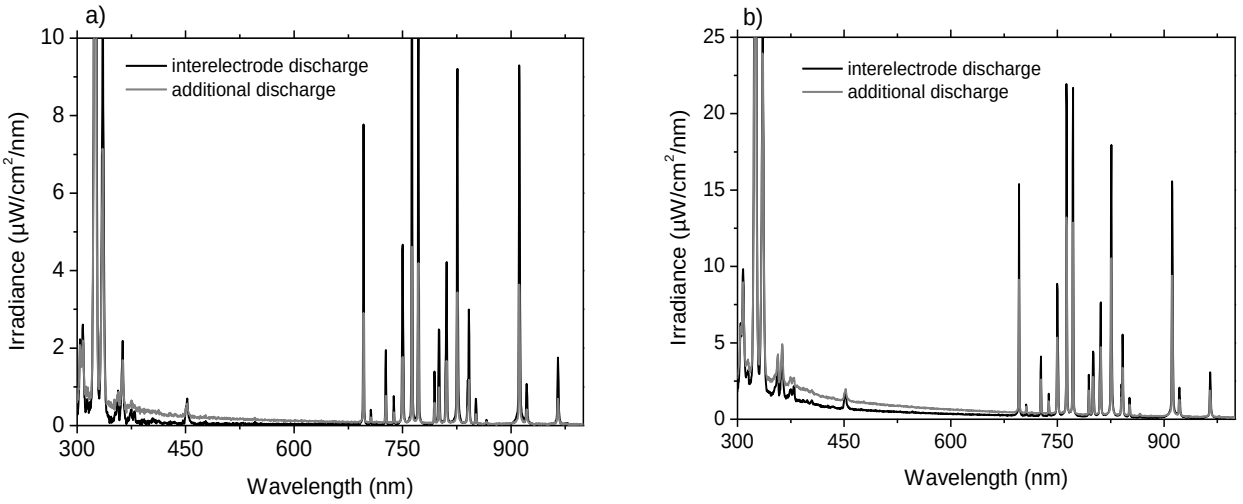

Figure 7: Irradiance of the inter-electrode discharge and center additional discharge for 550 kHz frequency with a) a 2 mm gap and b) a 4 mm gap

Figure 7 compares irradiance between inter-electrode and additional discharge sample at center position for a driving frequency of 550 kHz with 2mm and 4 mm gaps. For 2 mm (Figure 7-a), the spectra are very different. The additional discharge shows a similar spectrum to RF-DBD whereas the inter-electrode discharge has a TDBD spectrum. However, for a 4 mm gap, the continuum is present in both discharge zones. Nevertheless, argon emissions remain intense in the inter-electrode gap whereas they are weak in the additional discharge when the electric field is lower.

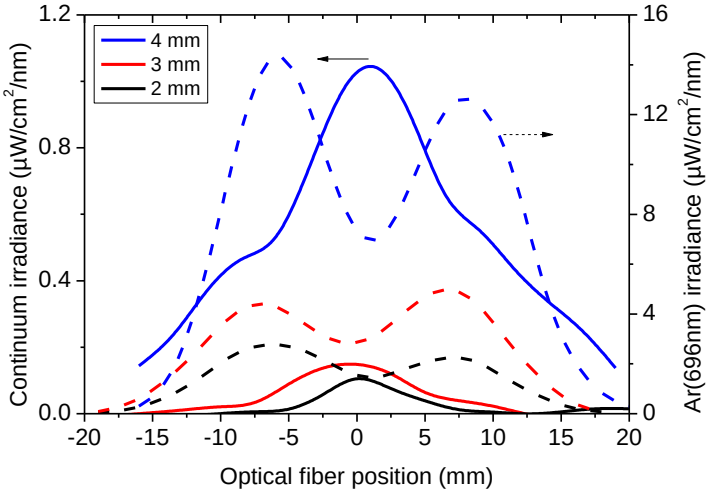

Figure 8: Irradiance of the continuum at 500 nm (full symbol) and of argon at 696 nm (open symbol) for 550 kHz along the position for 3 different gas gaps

In an attempt to discriminate the TDBD and RF-DBD discharge modes, spatially resolved irradiance was measured for the continuum at 500 nm and the argon emission at 696 nm for the different gas gaps. At 550 kHz, the results are plotted in Figure 8. The continuum was below the detection threshold at 1 mm gap and was only measurable in the center additional discharge with the 2 and 3 mm gaps. A drastic increase is observed between 3 and 4 mm and it was also observed between the electrodes, thus revealing that the continuum was present in the inter-electrode gap. This indicates an increase in electron density of the less-energetic electrons whereas the argon emission associated with energetic

electrons was still peaking in the inter-electrode gap. This mixed mode is characterized in the section below.

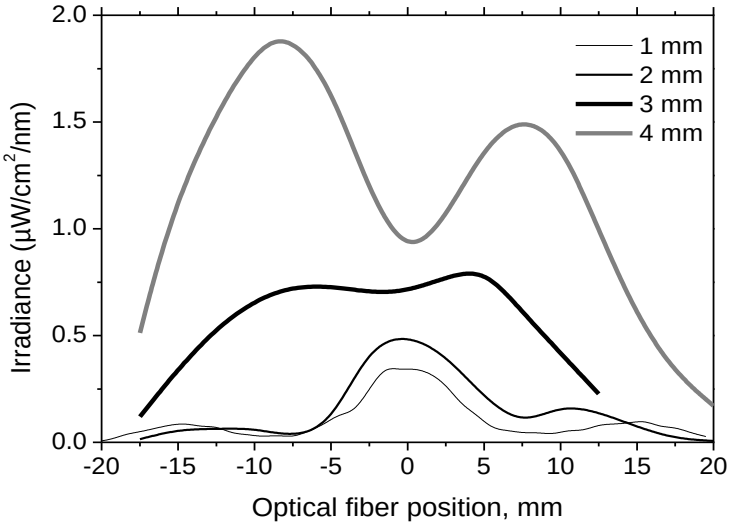

Figure 9: Irradiance profile of the continuum at 500 nm for 1.5 MHz and different inter-electrode gaps

At 1.5 MHz, with the 2 mm gas gap, the additional discharge at center splits into two discharges that are strongly linked to their inter-electrode discharges. When the gas gap is 3 and 4 mm, the discharge tends to become longer than the electrodes when the voltage is increased. Again, like for 550 kHz, the amplitude of the continuum at 1.5 MHz was plotted (Figure 9) along the position in different gas gaps. For 1 and 2 mm, the continuum is essentially located at the center, but from 3 mm and above it is gradually shifted under the electrodes, as is also the case for 1 mm gap and frequencies over 3 MHz. The irradiance profiles of the continuum are in agreement with the photographs given in Figure 5 for 1.5 MHz. For 1 mm gas gap, the continuum is more intense in the additional discharge at center where there is greater volume than at either end (Figure 5). At this frequency, for the voltage experimentally tested, the computed amplitude of oscillation of electrons is 3 mm [11]. Experimental observations suggest that RF discharge develops from this value upwards. With smaller gas gaps, the inter-electrode discharge struggles to develop as its intensity is too low.

3.3.2 Effect of voltage at 550 kHz for 4 mm gas gap

Photographs of the discharges obtained at voltages lower than those reproduced in Figure 6 are given in Figure 10.

At low voltage (0.8 kV), three additional RF discharges are observed although there is only little light emission in the inter-electrode gap. The shape of the discharge is the same than the one obtained at 1.5 MHz with a 1 mm gap. When the voltage is increased, the discharge gains intensity in the inter-electrode gap and light is mostly emitted from the middle of the gas gap, as also observed for RF-DBD as most of the ionization takes place in the bulk [6]. When the applied voltage is increased to 0.9 kV, the rise of the light concentration near the anode is associated with a Townsend discharge i.e. to a higher contribution of secondary electron emission. At 550 kHz, with a 4 mm gas gap and a voltage

amplitude of 1.05 kV, the inter-electrode discharge presents features similar to both RF-DBD and TDBD.

Applied voltage	550 kHz gas gap 4 mm
0.8 kV	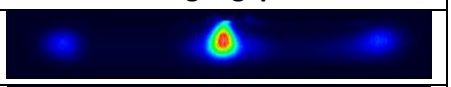
0.85 kV	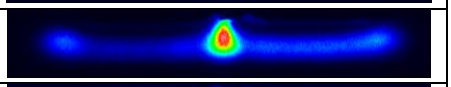
0.9 kV	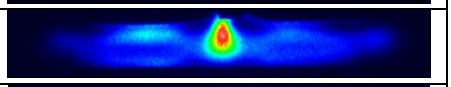
1.05 kV	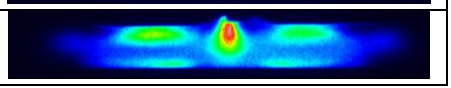

Figure 10: 3 ms exposure time imaging of discharge at 550 kHz with a 4 mm gap for various applied voltage

When a superposition of TDBD and RF-DBD is observed, if the power-supply voltage is decreased significantly, the TDBD contribution vanishes and only the RF discharge remains established. In any given configuration, decreasing the voltage has the same effect as increasing the frequency. It is the trapping of ions and electrons in the gas bulk that enables the RF discharge to be sustained, which is why the lowest applied voltage benefits the RF discharge. Furthermore, as the gas gap gets higher, the number of trapped ions also increases, which is why the RF discharge is easier to sustain.
For 4 mm gap with a 550 kHz frequency, an RF-DBD has a lower breakdown voltage than a TDBD, in agreement with the pattern observed at 1 mm gap when frequency is increased [11,19]. This finding can be explained as ion trapping benefits the formation of a space charges and minimizes electron losses at the walls [20]. Same phenomenon explains why RF-DBD is obtained at low-frequency, low voltage and high gas gap. When the applied voltage is high enough the ion trapping become less efficient. This enables the ions to reach the cathode, where they induce a secondary emission of electrons. Accordingly, the electron density gradient increases in the direction of the anode. For light emission to peak at the anode, the electric field has to be relatively homogeneous along the gas gap, which means there must be a limit to the ion density in the gap.

4. Conclusions

The transition from homogeneous Townsend-like DBDs (TDBD) to radio-frequency DBD (RF-DBD) modes was studied in an Ar/NH_3 mixture in a roll-to-roll configuration. The investigation focused on three parameters: frequency of the voltage applied to the electrodes, gas gap and voltage amplitude. These three parameters are complementary, as for a given gas and at a given pressure, they define the amplitude of charges motion due to drift and consequently the trapping rate of the charge in the gas. It increases with the applied voltage frequency and the gap and decreases with the applied voltage amplitude increase.
In roll to roll configuration, the transition from TDBD to RF-DBD is characterized by additional discharges that form outside the zone where the voltage is applied. In these zones, the gas gap is higher and the applied voltage is lower. Optical emission spectroscopy measurements showed that these

discharges emit a Bremsstrahlung continuum typical of RF-DBDs. Thus, for a 1 mm inter-electrode gas gap and a frequency up to 800 kHz, the inter-electrode discharge is a TDBD while the additional discharges are in RF-DBD. If the frequency or the inter-electrode gap are increased, the inter-electrode discharge becomes a RF-DBD and additional plasma disappeared. The presence of the two discharge mode is possible because (i) RF-DBD has a lower breakdown voltage than TDBD (ii) roll to roll configuration induces an increase of the gas gap on each side of the dielectric barrels that contain the electrode; the gas gap is higher, the electrical field is lower thus charges are trapped explaining the RF-DBD mode on the barrels side and the TDBD in between the electrodes.
Another feature is that the two modes are able to coexist at the inter-electrode gas gap, but not at the same time. This is observed for 550 kHz (low frequency limit of the transition TDBD/RF-DBD) and a gap of 3 mm or higher. When the voltage increases, the RF-DBD and the TDBD are successively observed, in the inter-electrode gap, for each half cycle. This transformation is attributed to the acceleration of ions to the cathode by higher electric field which increases the contribution of electron secondary emission.
Consequently, for given applied voltage frequency and amplitude, it is possible to tune the gas gap to obtain TDBD or RF-DBD. The important point is to which extend, electrons and ions are trapped in the gas gap.

5. Acknowledgements

The authors thank the French national research agency [*Agence Nationale de la Recherche* (ANR)] for part-funding the PREPA project (grant #ANR-09-BLAN-0043-03) and the "BATIR" FUI Project (F11211007U) financed by OSEO.

6. Bibliography

1 F. Massines, C. Sarra-Bournet, F. Fanelli, N. Naudé, N. Gherardi, Plasma Process. Polym. 2012, 9, 1041-1073
2 Starostin, S.A., et al., Plasma Sources Sci. Technol, 2009. 18(4): p. 045021.
3 Bonnin, X., et al, Eur. Phys. J. Appl. Phys., 2013. 64(1): p. 10901.
4 Liu, D.W., F. Iza, and M.G. Kong, Plasma Processes and Polymers, 2009. 6(6-7): p. 446-450.
5 Niemi, K., T. Gans, and D. O'Connell, Plasma Sources Sci. Technol, 2013. 22(3): p. 5.
6 T. Hemke, D. Eremin, T. Mussenbrock, A. Derzsi, Z. Donko, K. Dittmann, J. Meichsner, J. Schulze, Plasma Sources Sci. Technol., 2013, 22 015012
7 J. J. Shi and M. G. Kong in Appl. Phys. Lett.(2007), 90, 111502
8 B. Li, Q. Chen and ZW Liu in Appl. Phys. Lett.(2010), 96, 041502
9 Nozaki T and Okazaki K 2006, Pure Appl. Chem., 78, 1157–72
10 Kim D B et al, 2011, Phys. Plasma, 18, 043503
11 R. Bazinette, R. Subileau, J. Paillol, and F. Massines, Plasma Sources Sci. Technol. (2014) 23 035008
12 R. Bazinette, J. Paillol, and F. Massines, Plasma Sources Sci. Technol. 24 (2015) 055021 (9pp)
13 S. E. Alexandrov, N. McSporran and M. L. Hitchman, Chemical Vapor Deposition, Volume 11, Issue 11-12 (481-490)
14 A. Villermet, P. Cocolios, G. Rames-Langlade, F. Coeuret, J. L. Gelot, E. Prinz, F. Forster, Surf. Coat. Technol. 2003, 174, 899.
15 H. Caquineau, I. Enache, N. Gherardi, N. Naudé and F. Massines, J. Phys. D: Appl. Phys. 42 125201 (2009)
16 Arakoni R A et al 2007, J. Phys. D: Appl. Phys., 40 2476–90

17 Naudé N., Gherardi N., Es-Sebbar Et., Cambronne J-P., Massines F. (2004), HAKONE IX, Padova, Italy
18 Baguera N and Bogaerts A 2005 J. Appl. Phys. 97 123305
19 Nasser E 1971 Fundamentals of Gaseous Ionization and Plasma Electronics (New York: Wiley)
20 Liu D W, Shi J J and Kong M G 2007 Electron trapping in radiofrequency atmospheric-pressure glow discharges Appl. Phys. Lett. 90 041502